

## Thermodynamic analysis on the chemical vapor deposition process of Ta-C-H-Cl system

Hyun-Mi Kim<sup>a,b</sup>, Kwang Bo Shim<sup>b</sup>, Jung-Min Lee<sup>c</sup>, Hyung-Ik Lee<sup>c</sup> and Kyoong Choi<sup>a,\*</sup>

<sup>a</sup>Engineering Ceramic Center, Korea Institute of Ceramic Engineering Technology, Icheon 17303, Korea

<sup>b</sup>Division of Advanced Materials Science and Engineering, Hanyang Univ., Seoul 04763, Korea

<sup>c</sup>The 4<sup>th</sup> R&D Institute, Agency for Defense Development, Daejeon 34186, Korea

Carbon/carbon composites (C/C) have been widely studied in the aerospace field because of their excellent thermal shock resistance and specific strength at high temperature. However, they have the problems that is easily oxidized and deteriorated under atmospheric environment. In order to overcome these shortcomings, the CVD coating of ultra-high-temperature ceramics to C/C has become an important technical issue. In this study, thermodynamic calculations were performed to TaC CVD coating on C/C by FactSage 6.2 program. The Ta-C phase diagrams were constructed with the results of thermodynamic calculations in the Ta-C-H-Cl system. Based on the Ta-C phase diagram, the experimental conditions were designed to confirm the deposition of various phases such as TaC single phase, TaC + C and TaC + Ta<sub>2</sub>C by varying the composition of Ta/C ratio. The deposited films were found to be in good agreement with the predicted phases.

**Key words:** Ultra high temperature ceramics, Chemical vapor deposition, Tantalum carbide, Phase diagram.

### Introduction

Ultra-high-temperature ceramics (UHTCs) have been widely studied in extreme environments owing to their high-temperature (above 2000 °C) characteristics as next-generation aerospace materials [1-3]. In the aerospace field, the important factors are not only high-temperature stability but also weight reductions. Therefore, carbon-fiber-reinforced carbon matrix composites (C/C) have been widely used in aviation and space fields owing to their low density, high thermal conductivity, low coefficient of thermal expansion and high-temperature strength. However, C/C composites become oxidized by the reaction between carbon and oxygen over 500 °C in an air atmosphere [4, 5]. To improve the oxidation and ablation resistance of C/C composites in air, they must be coated with UHTCs such as tantalum carbide (TaC), zirconium carbide (ZrC) or hafnium carbide (HfC) [6-8].

Among UHTCs, TaC has an especially high melting point (~3950 °C), excellent thermal shock resistance and good chemical stability, making it a promising coating material to realize oxidation and ablation resistance for hypersonic vehicles (ICBM) and nozzles of aircraft engines [1, 7]. Because the sintering temperature of TaC is generally above 2700 °C, pressurized sintering techniques such as hot pressing

(HP) [9], hot isostatic pressing (HIP) [10] and spark plasma sintering (SPS) [11] can be used to lower the sintering temperature. However, these methods do not typically lead to high densification due to residual pores, and they still require a high temperature above 1900 °C. CVD techniques could be an alternative approach to produce high-quality TaC [6, 12] that is economically favorable and chemically compatible with C/C.

CVD coatings are especially effective tools for the uniform deposition of TaC on large and complicated C/C components. However, designing a CVD apparatus remains difficult with respect to the reproducibility of experiments because the gaseous chemical reactions between the Ta source and the hydrocarbon can be greatly affected by the gas flow inside the reaction chamber. Chen et al. proposed that the deposition of TaC could be dominated by surface kinetics at 800 °C and diffusion kinetics at 1200 °C and that subsequently the morphological evolution could be predicted on the basis of preferred orientations [6, 7]. Xiong et al. found that the sample positions within the hot zone region could affect the phases and morphologies of the deposited TaC layers [13].

Numerous efforts to find appropriate process conditions in TaC CVD have been carried out. Nevertheless, thermodynamic analyses of TaC CVD have rarely been reported thus far. Kim et al. recently investigated the effects of H/Cl and Ta/C ratios on the deposition phases in a Ta-C-Cl-H system and suggested a phase diagram predicting the deposition phases with Ta/C and

\*Corresponding author:  
Tel : +82-31-645-1456  
Fax: +82-31-645-1493  
E-mail: knchoi@kicet.re.kr

pressure variables [14]. Thermodynamic calculations for the CVD process are extremely important to understand the influence of the deposition parameters on the phases. By predicting the deposition phases using a thermodynamic analysis, an efficient and reproducible CVD process could be guided with a phase diagram.

In this study, a phase diagram based on the results of thermodynamic calculations in a Ta-Cl-C-H system is proposed and confirmed with experimental results with Ta/C and H/Cl variables. In order to control the amount of TaCl<sub>5</sub> powder, a powder feeder and a sublimator with CH<sub>4</sub> and C<sub>3</sub>H<sub>6</sub> carrier gases were used to control the deposition conditions.

## Experimental

### Thermodynamic calculation

The equilibrium compositions in the TaCl<sub>5</sub>-C<sub>3</sub>H<sub>6</sub>-H<sub>2</sub> (H/C = 8) system and the TaCl<sub>5</sub>-CH<sub>4</sub>-H<sub>2</sub> (H/C = 42) system were calculated using the FactSage 6.2 program (Thermfact/CRCT and GTT-Technologies, Montreal, Canada and Herzogenrath, Germany). In total, 54 chemical species consisting of 45 gaseous species and nine condensed species were considered for the thermodynamic calculations of the phase diagrams. The selected temperature range was from 1100 to 1400 °C. The selected process pressure range was from 10 to 500 torr. Only condensed phases are considered for the phase diagrams, which were constructed with the pressure and the composition, Ta/C, as variables under isothermal conditions.

### Chemical vapor deposition process of tantalum carbide

The substrates for the TaC deposition process were prepared with C/C composite (Daeyang Industries Co.,

Ltd., Korea) in a disc shape (F = 25.4mm & T = 5 mm). The apparatus for the deposition was a hot-wall CVD system of the vertical type [15] which was connected to the lines of a MTS (methyltrichlorosilane, CH<sub>3</sub>SiCl<sub>3</sub>) bubbler for SiC coating and a TaCl<sub>5</sub> sublimator for TaC coating, as schematically shown in Fig. 1.

The thermal expansion coefficient (CTE) of TaC ( $6.3 \times 10^{-6}/^{\circ}\text{C}$ ) is much higher than that of the C/C composites ( $1 \sim 2 \times 10^{-6}/^{\circ}\text{C}$ ). Thus, the SiC layer was deposited as an intermediate layer approximately 30 μm thick before the TaC deposition step. SiC CVD was carried out at a hot zone temperature and pressure of 1300 °C and 100 torr, respectively, and the flow rate of H<sub>2</sub> was 5 slm with a dilution ratio (H<sub>2</sub>/MTS) of 8 for two hours. Mixed hydrogen gases containing 10% C<sub>3</sub>H<sub>6</sub> and 5% CH<sub>4</sub> were used as the carrier gases for the TaCl<sub>5</sub> powder, which was continuously supplied to the sublimator using a screw-type powder feeder equipped with a DC motor. The film morphologies and phases were investigated with a scanning electron microscope (JEOL, JSM-6701F), a transmission electron microscope (Tecnai, G2 F30 S-Twin) and an X-ray diffractometer (Rigaku, D/MAX-2500PC).

The values of H/C were fixed at 8 for the 10% C<sub>3</sub>H<sub>6</sub>-containing hydrogen gas and 42 for the 5% CH<sub>4</sub> -containing hydrogen gas. If the carrier gases are saturated with TaCl<sub>5</sub>, the Ta/C ratio can be controlled using the feeding rate. The sublimation rate of the TaCl<sub>5</sub> powder can be calculated from the saturated vapor pressures, P<sub>(s)</sub>, as expressed by the equation [16] below.

$$\ln(P_{(s)}/\text{atm}) = 42.180 - 11123T^{-1} - 3.2207 \ln T \\ 1.761 \times 10^4 T^{-2} \pm 0.024 \quad (1)$$

When the flow rate of the carrier gas was 500 sccm and the temperature of the sublimator was 205 °C, the maximum feeding rate of TaCl<sub>5</sub> was calculated and found to be 2.85 g/min, as shown in Fig. 2. If the

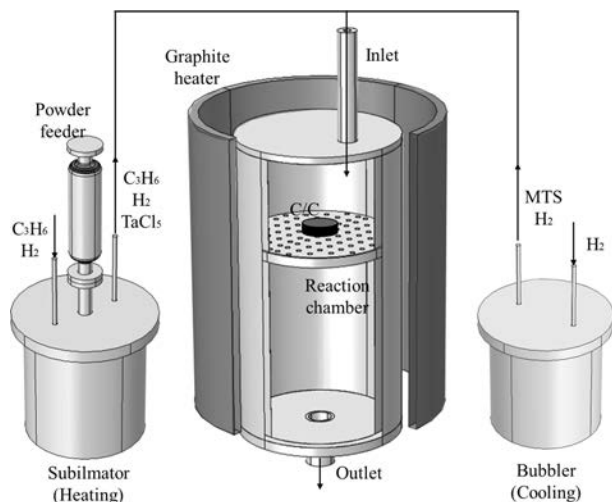


**Fig. 1.** Schematic diagram of the TaC deposition process used in the experiments.

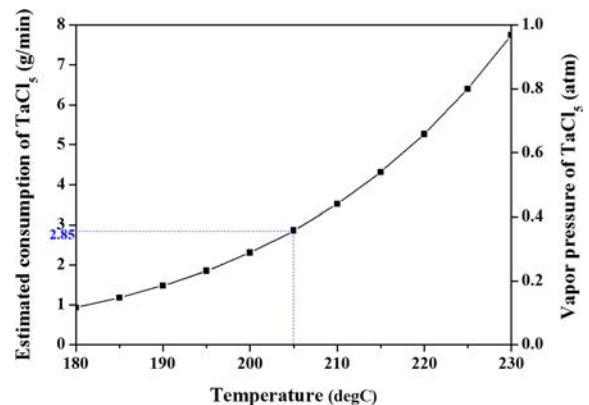


**Fig. 2.** Partial pressure of TaCl<sub>5</sub> powder with the temperature and corresponding consumption rate with saturated gas at a flow rate of 500 sccm.

feeding rate is higher than the maximum value, some powder could remain in the sublimator. For the reproducibility of the experiments, the feeding rate was held to less than 2.5 g/min.

## Results and Discussions

Phase diagrams for the  $\text{TaCl}_5\text{-C}_3\text{H}_6\text{-H}_2$  system with the variables of the pressure and Ta/C are shown in Fig. 2 when 10%  $\text{C}_3\text{H}_6$ -containing hydrogen is used as a reaction gas. The phase diagram of interest is focused on the Ta/C composition range of 0 to 2.5 owing to the practical growth conditions for the TaC film. The solid phases in the temperature range of 1100 to 1400 were C, TaC and  $\text{Ta}_2\text{C}$ . The single-phase region of TaC is wider at 1100 °C but the two-phase region of TaC and  $\text{Ta}_2\text{C}$  is expanded to the TaC region at a higher temperature. Therefore, the TaC single-phase region becomes narrower at 1400 °C.

On the other hand, when mixed hydrogen containing 5%  $\text{CH}_4$  is used as a reaction gas, the ratio of H/C becomes 42 and the phase diagrams for the deposition conditions change to those shown in Fig. 4. It can easily be confirmed that four solid phases of C, Ta, TaC and  $\text{Ta}_2\text{C}$  were found and that the total region is divided into five different regions consisting of two single-phase regions of TaC and  $\text{Ta}_2\text{C}$  and three double-phase regions of C + TaC, TaC +  $\text{Ta}_2\text{C}$ , and Ta +  $\text{Ta}_2\text{C}$ . In comparison with Fig. 3, a single-phase region of  $\text{Ta}_2\text{C}$  and a double-phase region of Ta +  $\text{Ta}_2\text{C}$  were also noted. In addition, a single-phase region of TaC appears in a very narrow region where Ta/C = 1.

The deposition of the TaC single phase in this system is expected to be very difficult.

The four different conditions used to assess the phase diagrams with the experimental data are denoted as Ta-1 to Ta-4 in Fig. 2(b) and Fig. 3(b). The Ta-1 and Ta-2 conditions only differed in terms of the  $\text{TaCl}_5$  feeding rate; Ta-1 is located in the TaC + C region and Ta-2 is in the TaC single-phase region. Ta-3 and Ta-4 are different only in terms of the gas flow rate and the feeding rate of  $\text{TaCl}_5$ , with the amount of reaction gases doubled in Ta-4. Due to the low content of carbon in the reaction gas in Ta-3, the feeding rate of  $\text{TaCl}_5$  was almost a quarter of that of Ta-1. All experimental conditions are summarized in Table 1.

The microstructures of the coating layers of the four experimental conditions above are shown in Fig. 5. Thick SiC layers of more than 20  $\mu\text{m}$  were deposited before the TaC CVD process. In Figs. 5(a) and 5(b),

**Table 1.** Four experimental conditions for the TaC deposition process.

	Ta-1	Ta-2	Ta-3	Ta-4
Temperature	1200 °C			
Pressure	100 Torr			
Time	2.5 hrs			
Gas flow rate	500 sccm		1 slm	
Process gas	10% $\text{C}_3\text{H}_6$ + 90% $\text{H}_2$		5% $\text{CH}_4$ + 95% $\text{H}_2$	
Ta/C	0.84	1.13	1.65	1.58
Predicted phases	TaC + C	TaC	TaC + $\text{Ta}_2\text{C}$	TaC + $\text{Ta}_2\text{C}$

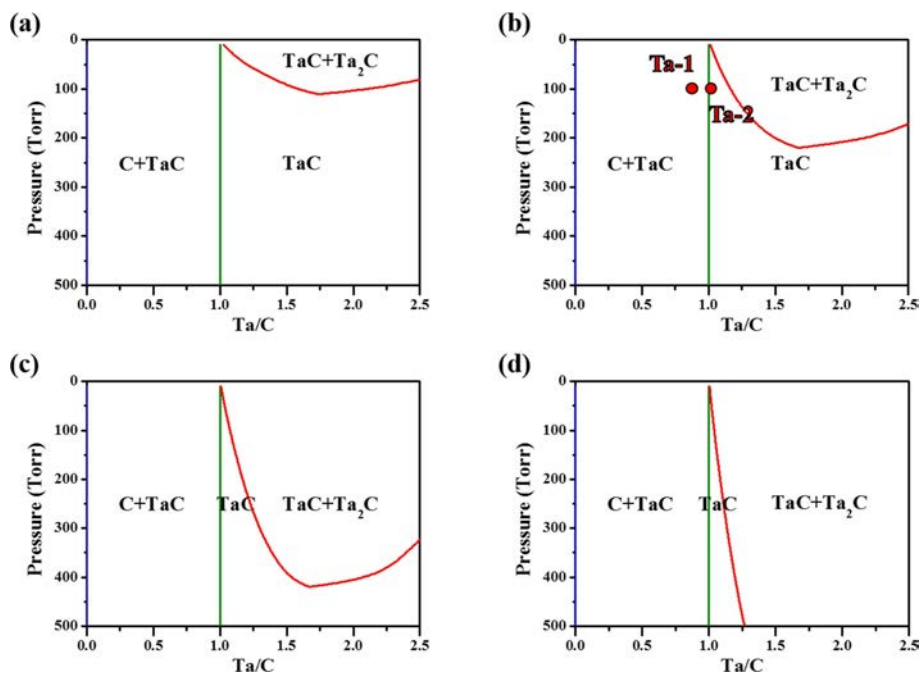


**Fig. 3.** Thermodynamic phase diagrams of H/C = 8 at (a) 1100 °C, (b) 1200 °C, (c) 1300 °C and (d) 1400 °C.

coating layers approximately 5  $\mu\text{m}$  thick were observed in Ta-1 and Ta-2 conditions, with surface morphologies of a cauliflower-like structure obtained, as reported elsewhere [12, 13]. A coating layer about 100 nm thick was found in the Ta-3 condition, as shown in Fig. 5(c). This carbide layer was attributed to the low feeding rate of  $\text{TaCl}_5$  and the higher activation energy for the dissociation of  $\text{CH}_4$ . The activation energy levels for

the dissociation of  $\text{C}_3\text{H}_6$  and  $\text{CH}_4$  during the TaC CVD process are 137 kJ/mol [17] and 273 kJ/mol [18], respectively. Wang et al. considered the influence of the C source during the deposition process leading to carbide formation from halide sources. It was also confirmed that  $\text{CH}_4$  gas had a lower deposition rate than  $\text{C}_3\text{H}_6$  under the same process conditions [19]. For the enhancement of the deposition rate of the carbides,

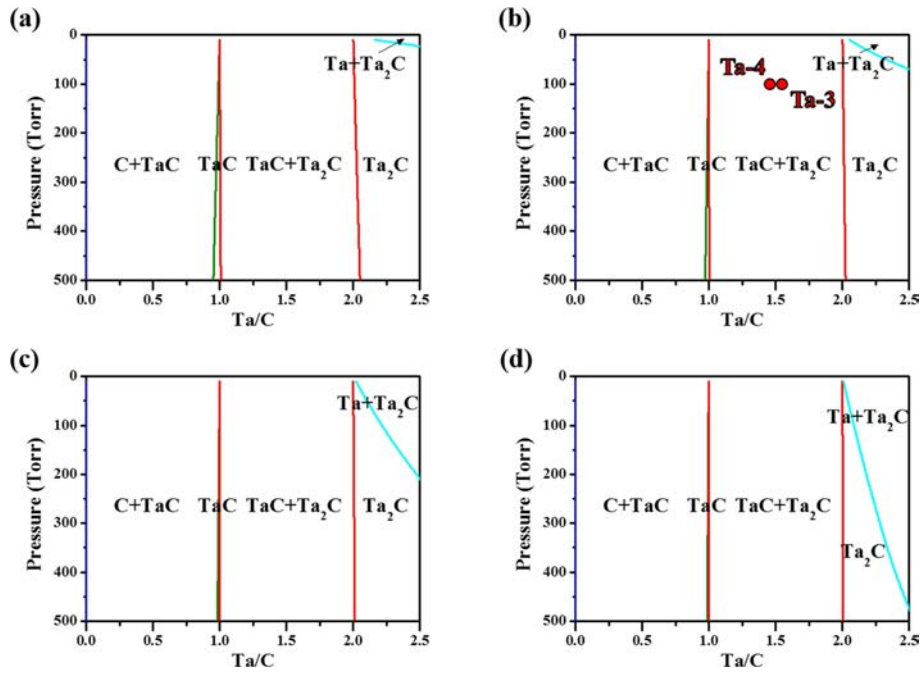


**Fig. 4.** Thermodynamic phase diagrams of  $\text{H}/\text{C} = 42$  at (a) 1100  $^{\circ}\text{C}$ , (b) 1200  $^{\circ}\text{C}$ , (c) 1300  $^{\circ}\text{C}$  and (d) 1400  $^{\circ}\text{C}$ .

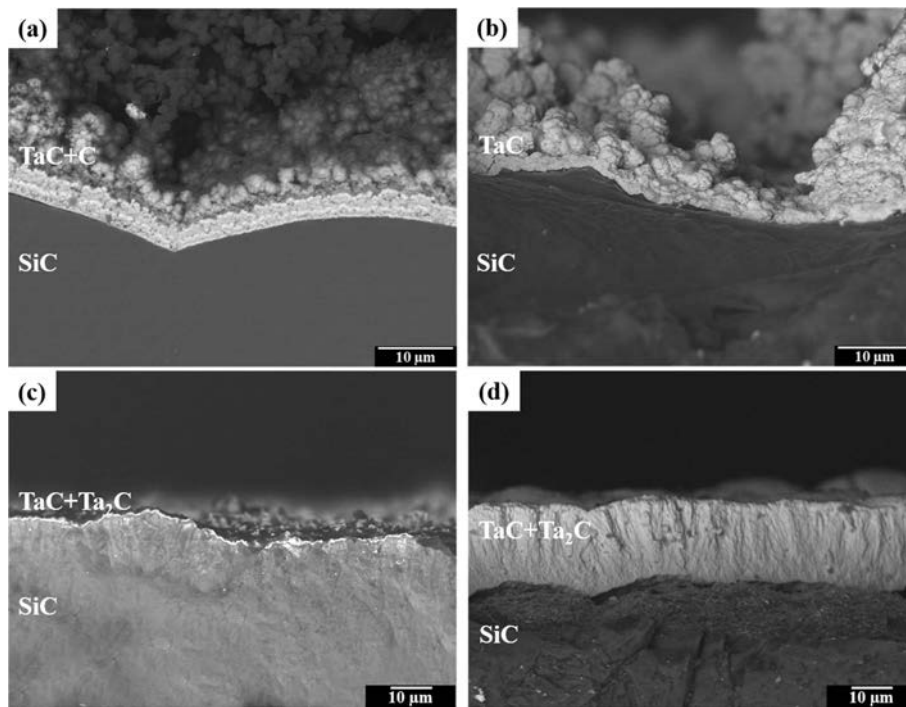


**Fig. 5.** SEM micrographs of cross-sectional views of TaC/SiC coated C/C specimens (a) Ta-1, (b) Ta-2, (c) Ta-3 and (d) Ta-4.

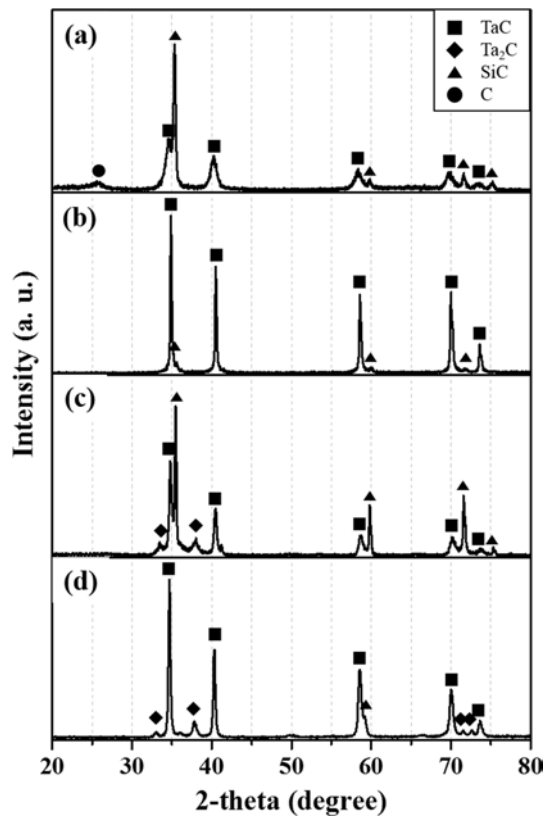


**Fig. 6.** XRD results for the TaC/SiC-coated C/C specimens of (a) Ta-1, (b) Ta-2, (c) Ta-3 and (d) Ta-4.

the flow rate of Ta-3 was doubled, which resulted in a thick coating layer more than 10  $\mu\text{m}$  thick in the Ta-4 condition.

XRD analyses were conducted to identify the phases in the deposited layers, as shown in Fig. 6. In the Ta-1

sample, TaC, SiC and a small amount of C phase were found. Only the TaC and SiC peaks were found in the Ta-2 specimen, and no carbon peaks were noted. The strong peaks of TaC relative to the SiC peaks reflect the high crystalline properties of TaC in Ta-2. TaC as well as Ta<sub>2</sub>C peaks were confirmed in Ta-3 and Ta-4. The lower intensity of the SiC peak in Ta-4 could be related to the thick coating layer of Ta-C compounds in the SiC layer. It was confirmed by an XRD analysis that the deposited phases precisely coincide with the predicted phases from the phase diagrams.

TEM analyses results for the Ta-1, Ta-2, and Ta-4 specimens are shown in Fig. 7. Figure 7(a) shows the microstructure of the TaC + C layer in Ta-1, where TaC nano-crystals of several nanometers are dispersed in the amorphous carbon matrix. Figure 7(d) shows an HR-TEM image and a SAED pattern of the samples shown in Fig. 7(a). A diffraction ring of amorphous carbon is formed at the inner-most position, and TaC diffraction rings which correspond to the FCC-rock salt structure of the (111), (200), (220), (311) and (222) crystal planes are present. Figure 7(b) shows the microstructure of the TaC layer in Ta-2, which is composed of TaC crystals on the micrometer scale. The SAED pattern in Fig. 7(e) appears to be a pattern from the TaC [112] zone axis. Figure 7(c) shows that the Ta-4 sample is composed of elongated crystals of sub-micron sizes. The grain boundaries are not clearly defined in their HR image due to their thickness, but the SAED pattern of the TaC and Ta<sub>2</sub>C crystal in Fig. 7(f) is obtained from the TaC [011] and the Ta<sub>2</sub>C [011] zone axis.

The morphologies of the TaC compound films were highly dependent on the precursor composition of Ta/C

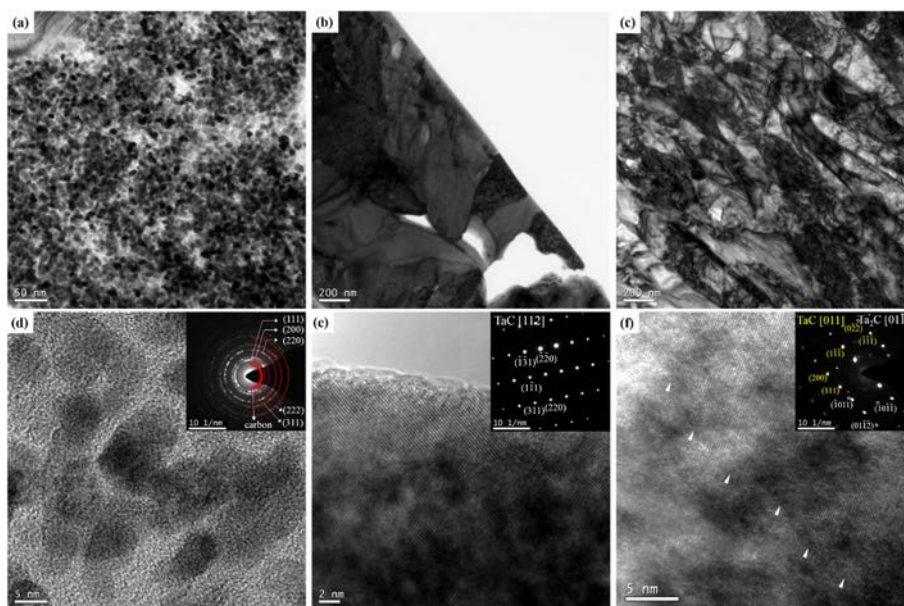


**Fig. 7.** TEM micrographs of TaC layers cut from (a) Ta-1, (b) Ta-2 and (c) Ta-4 specimens by FIB and corresponding high-resolution images and SAED patterns of (d) Ta-1, (e) Ta-2 and (f) Ta-4. The arrows in (f) show the grain boundary between the TaC and Ta<sub>2</sub>C crystals.

and H-Ta in the system. The film morphologies were believed to be the results of nucleation and grain growth. Therefore, the mechanism of nucleation and grain growth of the films is thought to depend on the composition of TaC, C and Ta<sub>2</sub>C. Several growth mechanisms have been proposed in relation to microstructural changes of TaC CVD thus far [6, 7, 20, 21]. The presence of nanocrystalline TaC crystals in the amorphous carbon matrix in Ta-1 is similar to the microstructure of Hf(Ta)C observed by Li et al. [22]. They proposed a model of the nucleation and growth of supersaturated TaC crystals in an amorphous carbon matrix. The growth mechanism of the Ta-2 sample is difficult to discern because the growth step had not proceeded sufficiently. However, it is considered to be the initial stage of columnar growth, as suggested by the evolutionary selection rule [23]. In the Ta-4 sample, TaC and Ta<sub>2</sub>C crystals appear to coexist, and the film growth is determined by the repetitive nucleation and growth of the two crystals. The TaC phase has an equiaxed morphology while the Ta<sub>2</sub>C phase has an elongated shape [20, 21], and the resulting morphologies of the film showed conglomerated crystals of TaC and Ta<sub>2</sub>C.

With respect to the anti-oxidation and anti-ablation properties of the deposition layer, the optimum conditions for the TaC film could be predicted and tailored by the phase diagram proposed in this study. The ablation characteristics of the films are known to be critically affected by their compositions and microstructures [7, 24, 25]. Thus, efforts to elucidate the relationship between the morphologies and compositions and the properties of the films should be made in near future.

### Conclusions

Thermodynamic analysis on CVD process in Ta-C-H-Cl system was carried out to predict the deposited phases by FactSage6.2. The phases and compositions were experimentally confirmed with a hot-wall CVD apparatus. The morphologies of the films were highly dependent on the composition of TaC, C and Ta<sub>2</sub>C.

### Acknowledgements

This work was supported by the Korean government (Ministry of Trade, Industry and Energy, MOTIE, and

Defense Acquisition Program Administration, DAPA) through Institute of Civil-Military Technology Cooperation.

### References

1. S. Tang and C. Hu, *J. Mat. Sci. Tech.*, 33 (2017) 117-130.
2. E. Wuchina, E. Oplia, W. Fahrenholtz and I. Talmy, *Electrochem. Soc. Interface*, 16 (2007) 30-36.
3. W. Fahrenholtz and G. Hilmas, *Scripta Mater.*, 129 (2017) 94-99.
4. V.Z.H. Shemet, A.P. Pomytkin and V.S. Neshpor, *Carbon*, 31 (1993) 1-6.
5. M.P. Bacos, *J. Phys. IV*, 3 (1993) 1895-1903.
6. Z. Chen, X. Xiong and Y. Long, *Appl. Surf. Sci.*, 257 (2011) 4044-4050.
7. Z. Chen, X. Xiong, G. Li, W. Sun and Y. Long, *Appl. Surf. Sci.*, 257 (2010) 656-661.
8. Q. Liu, L. Zhang, J. Liu and Y. Wang, *Inorg. Mater.*, 46 (2010) 1208-1213.
9. X. Zhang, G.E. Hilmas, W.G. Fahrenholtz and D.M. Deason, *J. Am. Ceram. Soc.*, 90 (2007) 393-401.
10. R.A. Morris, B. Wang, L.E. Matson and G.B. Thompson, *Acta Mater.*, 60 (2012) 139-143.
11. E. Khaleghi, Y. Lin, M.A. Meyers and E.A. Olevsky, *Scripta Mater.*, 63 (2010) 577-580.
12. Y. Long, A. Javed, J. chen, Z. Chen and X. Xiong, *Mater. Lett.*, 121 (2014) 202-205.
13. X. Xiong, Z. Chen, B. Huang, G. Li, F. Zheng, P. Xiao and H. Zhang, *Thin Solid Films*, 517 (2009) 3235-3239.
14. H.M. Kim, K. Choi, K.B. Shim, N.C. Cho and J.K. Park, *Kor. J. Mater. Res.*, 28 (2018) 75-81.
15. J.-W. Seo, J.-W. Kim, K. Choi and J.-H. Lee, *J. Korean Phys. Soc.*, 68 (2016) 170-175.
16. D. R. Sadoway and S. N. Flengas, *Can. J. Chem.*, 54 (1976) 1692-1699.
17. C. Lu, L. Cheng, L. Zhang and C. Zhao, *New Carbon Mater.*, 25 (2010) 35-40.
18. E. F. Arefeva and P. A. Tesner, *Solid Fuel chem.*, 5 (1977) 113-116.
19. Y. Wang, Q. Liu, L. Zhang and L. Cheng, *J. Am. Ceram. Soc.*, 91 (2008) 1249-1252.
20. K. Hackett, S. Verhoef, R. A. Cutler and D. K. Shetty, *J. Am. Ceram. Soc.*, 92 (2009) 2404-2407.
21. S. Dipietro, E. Wuchina, M. Opeka, K. Buesking, J. Spain, and L. Matson, *ECS trans.*, 14 (2007) 143-150.
22. Z. Li, Y. Wang, X. Xiong, X. Li, Z. Chen and W. Sun, *J. Alloy. Comp.*, 705 (2017) 79-88.
23. A.D.W. DRIFT, *Philips Res. Repts.*, 22 (1967) 267-288.
24. Y.L. Wang, X. Xiong, G.D. Li, X.J. Zhao, Z.K. Chen and W. Sun, *Surf. Coat. Technol.*, 206 (2012) 2825-2832.
25. Y.J. Lee and H.J. Joo, *Surf. Coat. Technol.*, 180-181 (2004) 286-289.